PNAS RESEARCH ARTICLE | BIOCHEMISTRY OPEN ACCESS

APC couples neuronal mRNAs to multiple kinesins, EB1, and shrinking microtubule ends for bidirectional mRNA motility

Sebastian J. Baumann[a], Julia Grawenhoff[a], Elsa C. Rodrigues[a], Silvia Speroni[a], Maria Gili[a], Artem Komissarov[a], and Sebastian P. Maurer[a,b,1]

Edited by Ronald Vale, HHMI - Janelia Farm Research Campus, Ashburn, VA; received July 5, 2022; accepted November 8, 2022

Understanding where in the cytoplasm mRNAs are translated is increasingly recognized as being as important as knowing the timing and level of protein expression. mRNAs are localized via active motor-driven transport along microtubules (MTs) but the underlying essential factors and dynamic interactions are largely unknown. Using biochemical in vitro reconstitutions with purified mammalian proteins, multicolor TIRF-microscopy, and interaction kinetics measurements, we show that adenomatous polyposis coli (APC) enables kinesin-1- and kinesin-2-based mRNA transport, and that APC is an ideal adaptor for long-range mRNA transport as it forms highly stable complexes with 3′UTR fragments of several neuronal mRNAs (APC–RNPs). The kinesin-1 KIF5A binds and transports several neuronal mRNP components such as FMRP, PURα and mRNA fragments weakly, whereas the transport frequency of the mRNA fragments is significantly increased by APC. APC–RNP-motor complexes can assemble on MTs, generating highly processive mRNA transport events. We further find that end-binding protein 1 (EB1) recruits APC–RNPs to dynamically growing MT ends and APC–RNPs track shrinking MTs, producing MT minus-end-directed RNA motility due to the high dwell times of APC on MTs. Our findings establish APC as a versatile mRNA-kinesin adaptor and a key factor for the assembly and bidirectional movement of neuronal transport mRNPs.

mRNA transport | microtubule cytoskeleton | kinesin | end binding proteins

Significance

Hundreds of different mRNAs are distributed by bidirectional, motor-protein-driven transport throughout axons and dendrites to provide templates for the assembly of local protein networks. This enables the neuron to configure cellular domains for specialized functions. Here, we provide mechanistic insights explaining how motor proteins, microtubule-associated proteins, RNA-binding proteins, and different mRNA fragments containing mRNA-localization signals self-assemble into functional mRNA transport complexes. Our results show that the microtubule-associated protein APC forms highly stable complexes with mRNAs, which can be processively transported by two different kinesin motor proteins. APC's high dwell times further enable tracking of shrinking microtubule ends, which together with plus-end-directed kinesin-based mRNA transport results in bidirectional mRNA motility.

The spatial control of gene expression via local translation of mRNAs is an essential prerequisite for the maintenance of cell polarity (1, 2), cell development, cell motility (3, 4), and the cotranslational assembly of protein complexes (5). In mammalian neurons, hundreds of mRNAs need to be distributed via microtubule (MT) -dependent, motor protein-driven transport in the form of small packages (6, 7) into a complex network of dendritic branches and the axon until the finest filopodia tips (8–10). As cells control intracellular cargo distribution through a combination of MT-associated proteins (MAPs) and MT post-translational modifications (PTMs) which enable or block the activity of distinct motors (11–13), it is expected that the complete localization process of an mRNA requires either several different adaptors for different motors or a versatile adaptor that can bind several motors (14). For instance in *Xenopus laevis*, a combination of a kinesin-1 and a kinesin-2 motor is required to localize Vg1 mRNA (15).

Arriving at a destination such as filopodia (16) or axonal branch points (17), mRNAs further need to be deposited or "anchored" at cellular structures of the cell cortex at locations where the encoded protein is needed. To date, a major mechanism known to deposit polarity factors at cell cortical elements is microtubule end-binding protein (EB)-dependent MT plus-end-tracking (18–20). MT plus-end-tracking creates transient density waves of plus-end-tracking proteins around polymerizing MT ends (21), and these high local concentrations are thought to drive the formation of polarity factor complexes at the cortex (22, 23). Hence, the question arises whether a mechanism exists that enables mRNA deposition at the cortex, in a similar way as for protein deposition, through MT plus-end–tracking-dependent, concentration-driven complex assembly. While a trailing of mRNPs behind polymerizing MT ends has been observed in axonal growth cones (16), a mechanism that could enable mRNP MT plus-end-tracking or trailing remains unknown.

Identifying a versatile adaptor which on the one hand specifically recognizes localization elements of mRNAs and on the other hand can also bind to different kinesins and eventually EB proteins would close a major gap in our understanding of how mRNPs could be distributed in mammalian cells. While we identified adenomatous polyposis coli (APC) as an mRNA adaptor that directly binds G-rich 3′UTR elements and the kinesin-2 KIF3AB-KAP3 ("KIF3ABK") with high affinities (24), more evidence exists from methods not proving direct interactions which hints toward an alternative, kinesin-1-based transport route for APC (25). This is of high interest, as the kinesin-1 KIF5 was long thought to be a major motor for mRNP transport in different mammalian cell types (26–28) but a minimal adaptor sufficient to couple mRNAs to KIF5 is not known. Further, APC interacts

Author contributions: S.P.M. designed research; S.J.B., J.G., and S.S. performed research; E.C.R., S.S., M.G., and A.K. contributed new reagents/analytic tools; S.J.B., J.G., S.S., and S.P.M. analyzed data; and S.J.B., J.G., and S.P.M. wrote the paper.

The authors declare no competing interest.

This article is a PNAS Direct Submission.

[1]To whom correspondence may be addressed. Email: sebastian.maurer@crg.eu.

This article contains supporting information online at https://www.pnas.org/lookup/suppl/doi:10.1073/pnas.2211536119/-/DCSupplemental.

Published December 5, 2022.

with EB proteins (*SI Appendix*, Fig. S1*A*, (29)) and tracks polymerizing MT plus ends (30), which predicts that APC–mRNPs potentially localize to polymerizing MT ends. mRNP plus-end-tracking would be a previously unconsidered mechanism to concentrate mRNPs locally, which could promote concentration-driven mRNP remodeling or anchoring of mRNPs at cortical cell structures for subsequent local protein production.

Using a combination of biochemical in vitro reconstitutions with pure proteins and RNA fragments (31), in vitro motility assays, in vitro microtubule dynamics assays (32), and surface plasmon resonance (SPR) interaction measurements, we show that APC couples neuronal mRNAs to the kinesin-1 KIF5A and the MT plus-end-tracking protein EB1. This results in kinesin-1-driven, fast, and highly processive plus-end-directed APC–RNP motility and EB1-mediated concentration of APC–RNPs at MT plus ends. In addition, we found that lattice-diffusing APC–RNPs can track shrinking MT ends resulting in minus end-directed RNA motility. Thus, APC is a versatile adaptor that links multiple G-rich fragments from at least four different neuronal mRNA-3′UTRs to KIF3ABK, KIF5A, and EB1, enabling bidirectional mRNP movements and potentially permitting APC–RNPs to access a wide range of dendritic and axonal segments.

Results

KIF5 Transports APC–RNPs. Prompted by a published loss-of-function and co-IP study showing that mammalian KIF5A, KIF5B, and KIF5C interact with the APC C-terminus (25), we set out to test whether APC directly interacts with KIF5 and whether APC is sufficient to couple neuronal mRNAs to KIF5. As we have previously shown that APC directly links 3′UTR-mRNA fragments to the KIF3ABK trimer (24), this would expand the interaction repertoire of APC, establishing it as a versatile mRNA-motor adaptor. Using biochemical in vitro reconstitutions in combination with Total internal reflection fluorescence microscopy (TIRF-M) (31), we compared the ability of the purified full-length mouse KIF5AA homodimer and the mouse KIF3ABK trimer (KIF5AA, *SI Appendix*, Fig. S1*B*) to transport reconstituted complexes of APC and $\beta2tub_{wt}$ 3′UTR-mRNA fragments (APC–RNPs, *SI Appendix*, Fig. S1*C*) at experimental conditions in which APC is mostly dimeric and binds one RNA per APC monomer (24). We found that KIF5AA homodimers processively transport APC–RNPs (Fig. 1*A* and Movie S1) and that transported complexes readily contain both APC and $\beta2tub_{wt}$ RNAs (Fig. 1*B*). At identical RNA:APC ratios, KIF3ABK and KIF5AA transport identical amounts of RNA (Fig. 1*C*), but their motile behavior differs significantly. As a measure for the motile behavior of KIF5AA- and KIF3ABK-based mRNA transport complexes, we used the confinement ratio, which measures how efficient a displacement is in moving away from the initial position (33). The movement of KIF3ABK is less confined than that of KIF5AA (Fig. 1 *A* and *D*), which is reflected in short diffusive periods within tracks of KIF3ABK-mediated RNP transport (Fig. 1*A*). At the same time, KIF5AA-based RNP transport exhibited an almost 2-fold lower dwell time on MTs (Fig. 1*E*), and even though the velocity of KIF5AA-mediated transport is 33% higher (Fig. 1*F*), the total distance traveled is several μm shorter, establishing KIF3–APC complexes as the more processive mRNA transporter (Fig. 1*G*).

As shown previously (24), KIF3 has essentially no RNA binding activity under our experimental conditions. *Drosophila* KIF5, however, can directly bind U-rich elements (34). To test the specificity of KIF5–RNA interactions, we investigated whether mammalian KIF5AA could also transport a $\beta2tub_{wt}$ 3′UTR-mRNA fragment containing a high fraction of G residues (*SI Appendix*, Fig. S1*c*). We found that KIF5AA can transport this RNA as well (Fig. 1*H* and Movie S1), even though with a 5-fold reduced efficiency compared to complexes also containing APC (Fig. 1*I*). Comparing the velocities of $\beta2tub_{wt}$ RNA transport by KIF3ABK–APC, KIF5AA–APC, and KIF5AA (Fig. 1*F*) surprisingly revealed that KIF5AA-based transport in the absence of APC is the fastest RNA transport mode among the three options.

KIF5 motors were shown to interact with several neuronal transport mRNP components such as the RNA-binding proteins (RBPs) FMRP and PURα either directly or indirectly (28, 35). Inspired by the diversity of observed KIF5AA interactions, we next tested whether KIF5AA can also directly bind and transport other mRNP components such as the aforementioned canonical RBPs. As challenges with protein biochemistry forced us to work with mGFP-labeled RBPs, we compared their transport efficiency to mGFP-labeled APC. mGFP-FMRP and mGFP-PURα (*SI Appendix*, Fig. S1*D*) transport by KIF5AA was only detectable at concentrations ~10-fold*** above the concentration needed to observe robust APC–mGFP transport (Fig. 1 *J* and *L* and Movies S2 and S3). Given that a recent study observed a significantly higher association of FMRP with KIF5B vs. KIF5A in pull-down assays using murine brain lysate (Zhao et al., 2020), we also purified full-length, unlabeled KIF5BB (*SI Appendix*, Fig. S1*D*) and tested its ability to transport mGFP-FMRP. We found that besides KIF5AA, also KIF5BB is not able to transport mGFP-FMRP efficiently in vitro (Fig. 1*K*). The addition of active, full-length MAP7 (*SI Appendix*, Fig. S1 *D* and *E*), a known activator of KIF5 (36–38), could not increase the observed low FMRP transport efficiency. We hence conclude that the increased ability of KIF5B to pull FMRP from brain lysate (35) requires additional factors which were not present in our in vitro reconstitution assay and are yet to be identified.

Similar to the high velocity of KIF5AA-mediated RNA transport in the absence of APC (Fig. 1*F*), the transport velocity of FMRP was also significantly higher than that of APC (Fig. 1*M*), hinting toward a distinct transport mode of APC and APC–RNPs. These data further show that although KIF5AA can bind several neuronal transport mRNP components, its affinity to APC is likely orders of magnitude higher, positioning APC as the primary factor for neuronal mRNA-motor coupling among the investigated factors.

APC–RNA Complexes are Highly Stable. While the preceding data establish APC as a versatile, potential neuronal mRNP transport adaptor, it is not known how stable APC–RNA complexes are. Given that RNP complex stability is a crucial requirement for long-range transport processes, we aimed to shed light on APC–RNA interaction dynamics and affinities using SPR interaction kinetics. To this end, we purified an APC fragment containing a Twin-Strep-tag® and the basic MT-binding domain ("APC-basic", *SI Appendix*, Fig. S2*A*) and obtained four different minimal 3′UTR fragments comprising G-rich APC motifs (*SI Appendix*, Fig. S1*c*). Three of these fragments originate from mRNAs previously described as APC targets (β-actin, β2tub and Map1b) (39), whereas one fragment originates from the Camk2α mRNA 3′UTR which was not detected as an APC target previously but contains a G-rich structure (G-quadruplex) recognized by FMRP (40, 41). We first set out to measure the interaction kinetics of APC and $\beta2tub_{wtmin}$ RNA vs. APC and a control RNA ($\beta2tub_{mutmin}$ RNA), in which G residues were replaced with other nucleotides (*SI Appendix*, Fig. S1*C* and Fig. 2 *A* and *B*). While APC shows a moderate association rate to $\beta2tub_{wtmin}$ RNA (Fig. 2*A*), its dissociation rates using both a one-state and a two-state interaction model, are in the range of 10^{-2} to 10^{-4}/s (Fig. 2*A* and *SI Appendix*, Fig. S2*B*).

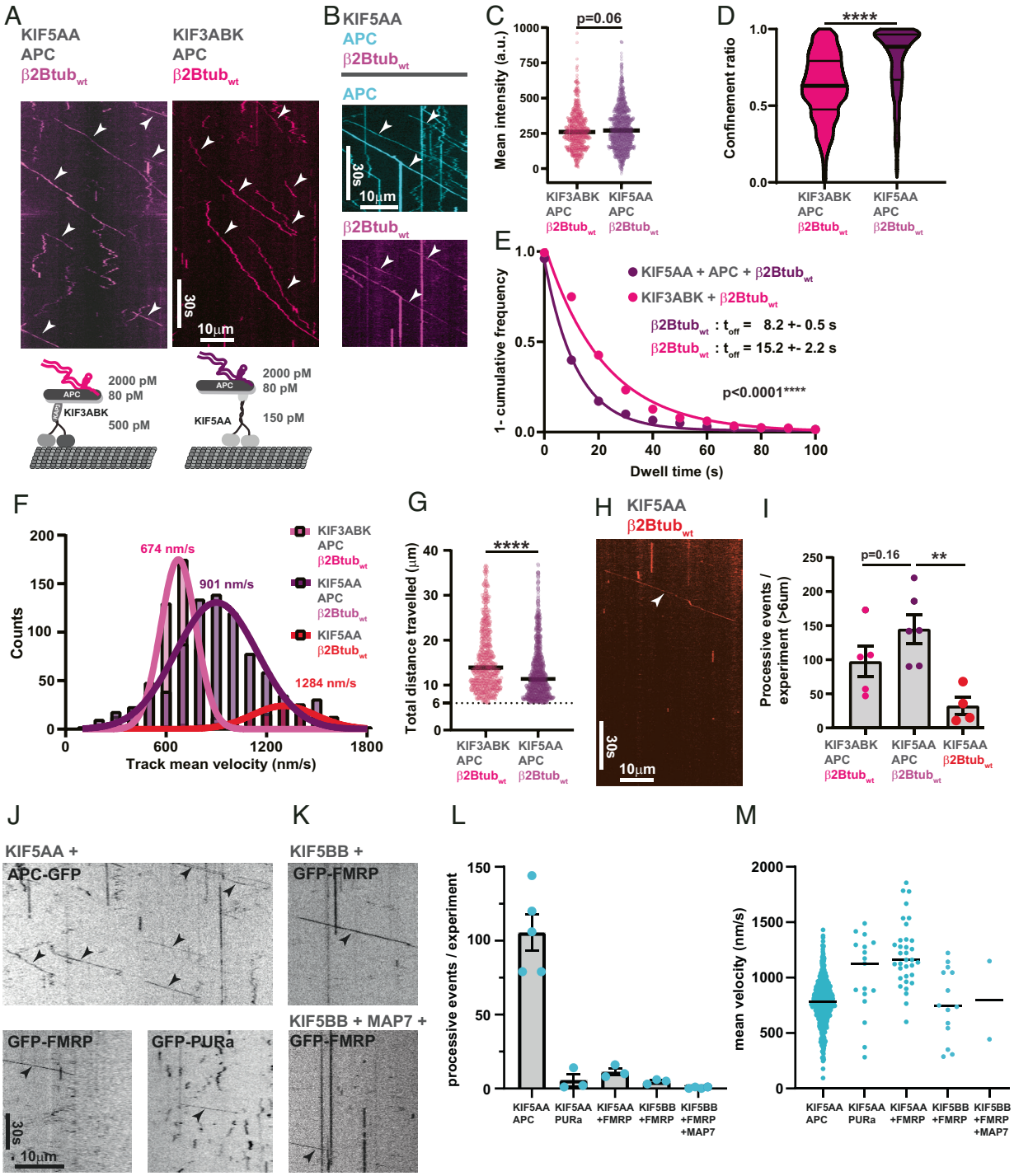

Fig. 1. APC links β2tub-RNA to kinesin-2 and kinesin-1 for processive transport. (*A*) KIF3ABK and KIF5AA transport APC/647-β2tub$_{wt}$ complexes. Kymographs showing comparable numbers of processive 647-β2tub$_{wt}$ transport events driven by kinesin-2 (pink) and kinesin-1 (magenta) in the presence of APC. Cartoons depict the components of each minimal transport system and indicate concentrations used for both systems. (*B*) 150 pM KIF5AA transports RNPs containing 80 pM APC–TMR and 2 nM 647-β2tub$_{wt}$. A kymograph showing multiple corun events of APC–TMR and 647-β2tub$_{wt}$ complexes, indicated by white arrowheads. (*C*) Quantification of 647-β2tub$_{wt}$ fluorescence mean intensities for KIF3ABK+APC+647-β2tub$_{wt}$ and KIF5AA+APC+647-β2tub$_{wt}$ transport complexes. (*D*) Violin plot depicting confinement ratio of processive β2tub$_{wt}$ run events for kinesin-2 (pink)- or kinesin-1 (magenta)-driven transport in the presence of APC. (*E*) Dwell times of 647-β2tub$_{wt}$ in the presence of KIF3ABK+APC or KIF5AA+APC. (*F*) Histogram showing mean velocities of processive β2tub$_{wt}$ run events for kinesin-2 (pink)- and kinesin-1 (magenta)-driven transport in the presence of APC as well as for kinesin-1-driven transport in the absence of APC (red). Pink, magenta and red curves represent Gaussian fits for mean velocity distributions (*G*) Scatter plot showing the total distance that 647-β2Btub$_{wt}$ RNAs travel in the presence of KIF3ABK+APC or KIF5AA+APC. (*H*) Kymograph showing the KIF5AA-driven 647-β2tub$_{wt}$ transport in the absence of APC. The cartoon depicts the components and indicates concentrations used in the experiment. (*I*) Quantification of processive β2tub$_{wt}$ run events for kinesin-2 (pink)- or kinesin-1 (magenta)-driven transport in the presence of APC as well as for kinesin-1 driven transport in the absence of APC (red). Since motor independent particles, containing only APC and RNA, diffuse along MTs for several micrometers, we only considered processive particles with a displacement of > 6 μm (*SI Appendix*Fig. S1*F*). Error bars indicate SEM. (*J*) Kymographs showing KIF5AA (150 pM)-mediated transport of APC-mGFP (80 pM), mGFP-FMRP (800 pM), and mGFP-PURα (800 pM). (*K*) Kymographs showing KIF5BB (150 pM)-mediated transport of mGFP-FMRP (800 pM) in the absence and presence of MAP7 (10,000 pM), respectively. (*L*) Quantification of APC-mGFP, mGFP-FMRP, and mGFP-PURα transport events at 150 pM KIF5AA and mGFP-FMRP transport at 150 pM KIF5BB in the absence and presence of MAP7, respectively. (*M*) Mean track velocities of APC-mGFP, mGFP-FMRP, and mGFP-PURα transport events. Median velocities are indicated. Statistical significance in *H* was evaluated with unpaired, two-tailed *t* tests and in *C*–*F* and *L* with unpaired Mann–Whitney tests. Horizontal bars in *C*, *E* and *L* represent the median. Horizontal bars in *D* represent median and quartiles.

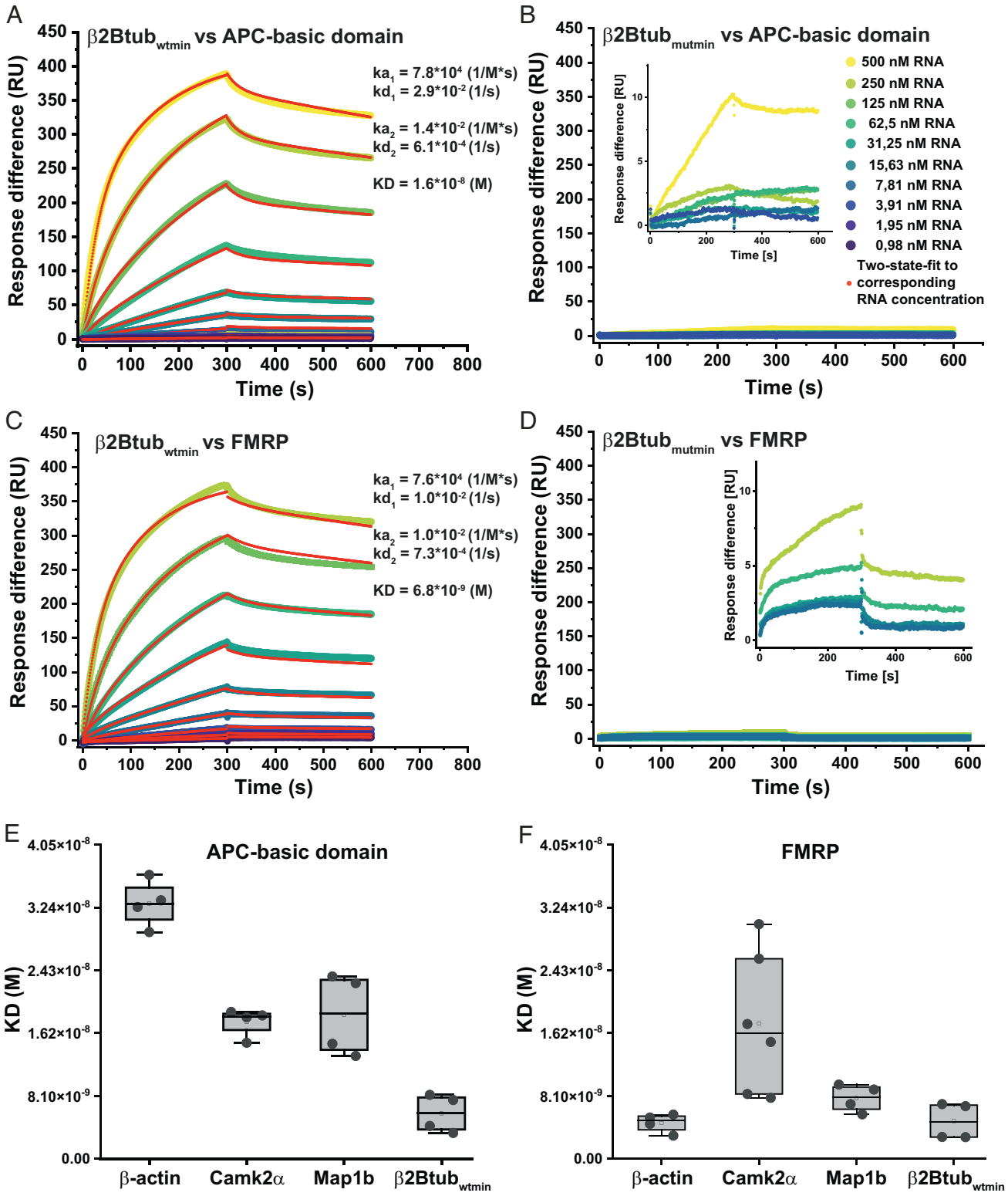

Fig. 2. APC-basic domain and FMRP bind G-rich target RNAs with high affinity. (*A* and *C*) Graphs generated from SPR experiments showing the binding kinetics (association and dissociation rates) of different concentrations of β2tub$_{wtmin}$ RNA and APC-basic or FMRP, respectively. Experimentally determined curves were fitted with a two-state binding model. (*B* and *D*) Graphs generated from SPR experiments showing the association and dissociation of different concentrations of β2tub$_{mutmin}$ RNA and APC-basic domain as well as FMRP, respectively. (*E* and *F*) Plot of APC and FMRP target RNA dissociation constants. Experiments were performed at least in duplicates with two technical replicates each.

APC–β2tub$_{wtmin}$ RNA complexes are hence stable for minutes and as such are suitable for longer transport processes needed to deliver mRNP packages to different locations within hundreds of micrometers long neurites. Confirming published TIRF-M and microscale thermophoresis data (24), there is essentially no interaction detectable between APC and the β2tub$_{mutmin}$ RNA.

FMRP binds G-rich sequences very similar to those recognized by APC, and their mRNA target pools at least partially overlap,

while the two proteins differ in their functions (27, 39, 42, 43). It is hence interesting to understand if both RBPs would compete for the same mRNAs, either for translation regulation or for the assembly of different mRNA transport complexes. Testing $\beta2tub_{wtmin}$ and $\beta2tub_{mutmin}$ RNAs binding to immobilized FMRP (*SI Appendix*, Fig. S2*A*) revealed an even higher affinity and similar low off rates of FMRP to $\beta2tub_{wtmin}$ RNA (Fig. 2*C*), in comparison to APC, while very little FMRP binding activity was detected for $\beta2tub_{mutmin}$ RNA (Fig. 2*D*), similar to APC.

We finally extended the SPR analysis to all four 3′UTR fragments. We found that both APC and FMRP bind all wild-type RNAs with nM-range affinities (Fig. 2 *A*, *C*, *E*, and *F* and *SI Appendix*, Fig. S2 *B*–*D*). The only difference was detectable for β-actin RNA (*SI Appendix*, Fig. S2*D*): here, SPR analysis was only possible with a narrower concentration range, reducing the confidence in the measured difference. We therefore conclude that FMRP and APC would likely compete for the same mRNA localization motifs, but note that seemingly small differences detected here could have a strong effect on mRNA transport. APC, for instance, binds β-actin RNA with 3-fold lower affinity than $\beta2tub_{wt}$ RNA. Still, we could show previously that this small difference is sufficient to almost entirely block β-actin mRNA transport in the presence of equimolar amounts of $\beta2tub_{wt}$ RNA (24).

KIF3 and KIF5 Do Not Act Synergistically during APC–RNP Transport. Having established APC as both a versatile but also efficient mRNA-motor adaptor, we next asked whether APC could employ KIF3 and KIF5 simultaneously. Such a mechanism could be beneficial, e.g., for super-processive long-range transport of mRNAs along the neuronal axon. Given that KIF3 binds the N-terminal ARM domain of APC via KAP3 (44), while KIF5 was reported to bind the C-terminus of APC (25) (*SI Appendix*, Fig. S1*A*), a cotransport scenario would be possible. We hence analyzed the motility of complexes containing APC-647 (*SI Appendix*, Fig. S3*A*) and RNA in the presence of either KIF3ABK (scenario 1), KIF5AA (scenario 3), or both kinesins (scenario 2) (Fig. 3*A*). Qualitatively, the addition of KIF5AA to KIF3ABK–APC–RNA complexes caused little difference in motile behavior (Fig. 3*B*, (scenario 2)) compared to KIF3ABK–APC–RNA motility (Fig. 3*B*, (scenario1)). The number of processive APC transport events did not increase significantly upon KIF5AA addition (Fig. 3*C*), indicating that the APC concentration was limiting in our experiments. Interestingly, while the velocity distribution of the two-motor scenario (Fig. 3*D*, (scenario 2)) was bimodal with peaks matching the velocities of KIF5AA- and KIF3ABK-based APC–RNA transport, addition of KIF5AA produced a confinement ratio distribution (Fig. 3*E*, (scenario 2)) very similar to that of the pure KIF5AA condition (Fig. 3*E*, (scenario 3)). The dwell times (Fig. 3*F*) and the total distance traveled (Fig. 3*G*) of the two-motor scenario (2) are intermediates between the pure KIF3ABK–APC–RNA scenario (1) and the pure KIF5AA–APC–RNA scenario (3). As an additional readout, we next analyzed the motile behavior of TMR-KIF3ABK which was present in scenarios 1 and 2. Qualitatively, the addition of KIF5AA to KIF3ABK–APC–RNA mixtures led to some faster KIF3ABK run events (Fig. 3*H*). Addition of KIF5AA further led to a reduction of the KIF3ABK dwell time, similar to what we observed for APC comparing scenarios 1 and 2 (Fig. 3 *I* and *F*). Also, the number of processive KIF3ABK tracks per experiment did not change significantly, as observed for APC (Fig. 3 *J* and *C*). As the data from Fig. 3 *H* and *I* indicated an effect of the presence of KIF5AA on KIF3ABK, we next aimed to simplify the experiment and compared solely the activity of KIF3ABK in the absence and presence of KIF5AA (Fig. 3*J* and Movie S4). While there were very little processive tracks observable for KIF3ABK, addition of KIF5AA increased processive run events of KIF3ABK, pointing at a direct high-affinity interaction of both motors, considering the pM-range concentrations used (Fig. 3*A*). Analyzing the KIF3ABK confinement ratio in response to KIF5AA addition, either in the presence of APC and RNA or not, showed an increase of KIF3ABK processivity in both cases (Fig. 3*K*). Also, the velocity of KIF3ABK increased quantitatively through the addition of KIF5AA (Fig. 3*L*). These experiments show that both kinesins are not likely engaged in simultaneous transport of APC, since the association of a single cargo with several motors is expected to decrease its detachment from the MT and thus increase its overall processivity. Also, the fact that the number of processive KIF3ABK events does not decrease by the addition of KIF5AA points in the same direction, as KIF3ABK is barely active on its own (Fig. 3*J*). Surprisingly, both motors can interact in the absence of any cargo, which causes KIF3ABK to adopt a more KIF5AA-like motile behavior, an effect we have also observed when analyzing APC motility (Fig. 3*D*). Due to the direct crosstalk between both kinesins, however, we do not know whether the altered APC motility is the result of both motors acting on APC, or if we observe the consequences of altered motor behavior that results from their direct interaction. These results prompted us to reinvestigate which APC domains are bound by the individual kinesin motors to understand better if both motors could act together during APC cargo transport.

Both Kinesins Bind and Transport the APC–ARM Domain. While the binding of the KIF3ABK trimer or KAP3 alone to the APC–ARM domain was shown with methods reporting direct interactions (24), binding of KIF5 to the APC C-terminus was only tested with methods that cannot discriminate between direct or indirect interactions (25). We hence purified an Alexa647-labeled C-terminal APC fragment ("APC-C", *SI Appendix*, Fig. S4*A*), containing the MT-binding region and the proposed KIF5 binding site, but lacking the APC–ARM domain. Comparing the motility of full-length APC with APC-C in the presence of unlabeled KIF5AA showed that the deletion of the ARM domain reduces processive APC transport events, while the number of diffusive events is increased (Fig. 4 *A*–*C*). Almost no KIF3ABK-mediated transport of APC-C was detected, underlining that this motor specifically recognizes the ARM region in the N-terminal domain of APC (Fig. 4 *A*–*C*). Of note, the velocity of KIF5AA-mediated APC-C transport is higher than the velocity of full-length APC transport (Fig. 4*D*). This observation led us to speculate that full-length APC might have multiple MT binding sites, which could lead to a transport mode in which APC continues to interact with the MT during transport. This could potentially reduce APC transport velocity but could also increase processivity.

As we would expect that a multivalent attachment of full-length APC to the MT lattice would increase its dwell time, we first tested whether the dwell times of full-length APC and APC-C differ. Since the number of processive events for APC-C is too low for further analysis, we took only diffusive full-length APC and APC-C events into account. To this end, we applied a tracking filter, allowing us to restrict the analysis to APC and APC-C tracks with a displacement between 1 and 7 μm, a distance characteristic for diffusing APC (24). Full-length APC shows a biphasic dwell time with either very short diffusion events of 2.3 s or approximately 10 times longer diffusion events of 26.3 s, indicating that it harbors at least two MT binding sites (Fig. 4*E*). In contrast to full-length APC, APC-C dwell time curves are best fitted with a monoexponential curve, exclusively showing higher turnover events of 2.5 s, which most likely result from a single MT-binding site. Considering

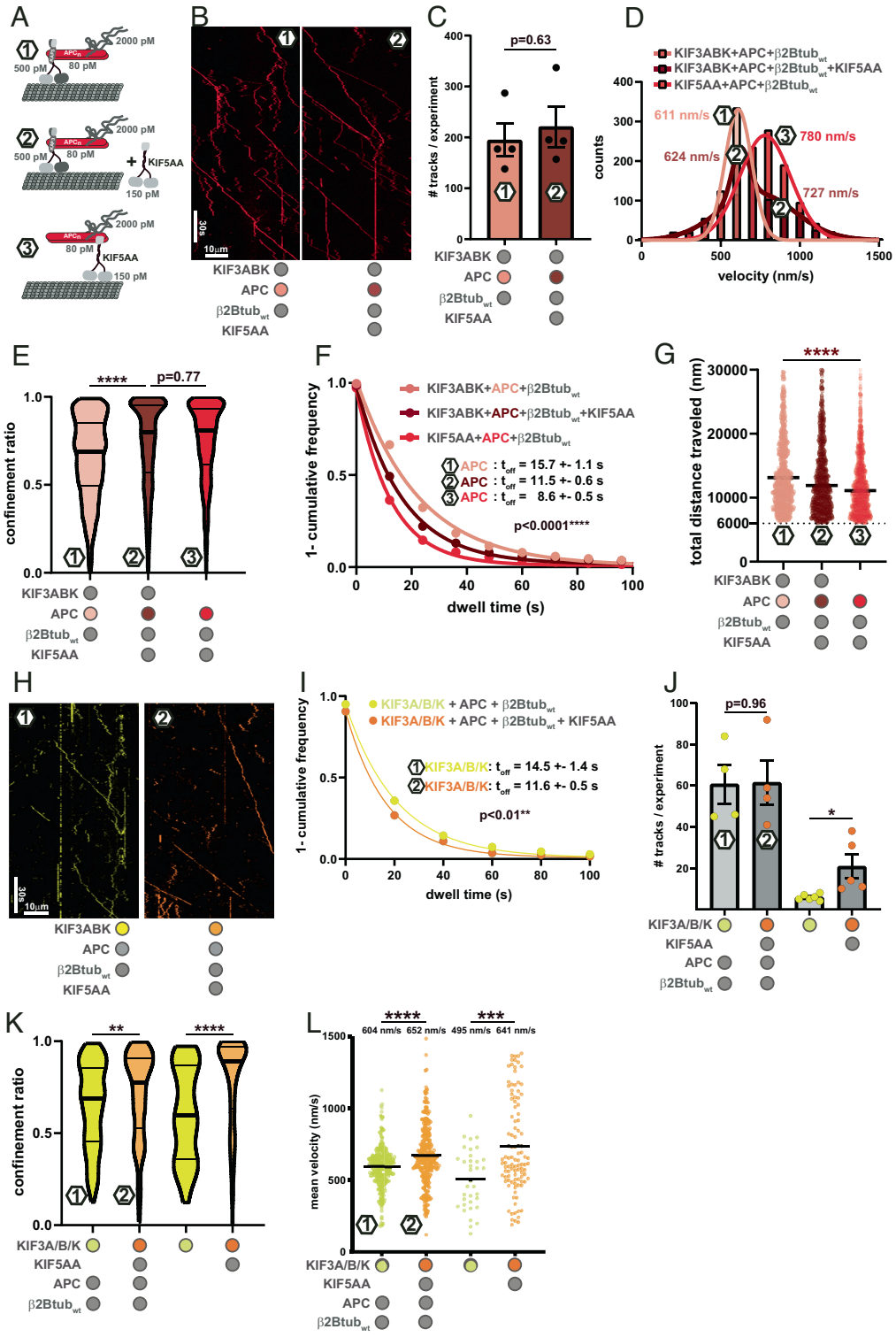

Fig. 3. Combined effect of KIF5AA and KIF3ABK on RNA transport (*A*) Cartoon depicting the experimental setup used to investigate the effect of kinesin motors on APC in different scenarios: 1) KIF3ABK+APC-647; 2) KIF3ABK+APC-647+KIF5AA; 3) APC-647+KIF5AA. Picomolar concentrations of components are indicated. (*B*) Kymographs showing APC-647 in the presence of β2tub$_{wt}$ and KIF3ABK (*Left*), or in the presence of β2tub$_{wt,}$ KIF3ABK and KIF5AA (*Right*). (*C*) Quantification of processive RNP transport events containing APC-647 in the presence of β2tub$_{wt}$ and KIF3ABK or in the presence of β2tub$_{wt,}$ KIF3ABK and KIF5AA, respectively. Statistical significance was evaluated with an unpaired, two-tailed *t* test. (*D*) Velocity distributions of APC-647 in the presence of KIF3ABK (1), KIF3ABK and KIF5AA (2), or KIF5AA (3). Velocity distribution of (1) and (3) were fitted with a Gaussian curve whereas (2) was fitted with the sum of two Gaussians. (*E*) Violin plot depicting the confinement ratio of transported APC-647 in conditions (1)(2) and (3). Statistical significance was evaluated with an ordinary one-way ANOVA test. (*F*) Dwell times of APC-647 in all three conditions. (*E* and *F*) Statistical significance was evaluated with a Kruskal-Wallis test. (*G*) Total distance traveled of APC-647 in all three conditions. Statistical significance was evaluated with an unpaired Mann–Whitney test. (*H–M*) Analysis of TMR-KIF3ABKAP in the three conditions. (*H*) Kymographs showing TMR-KIF3ABKAP in the presence of APC-Alexa-647 and β2Btub$_{wt}$ (*Left*), or with the addition of KIF5AA (*Right*). (*I*) Dwell times of TMR-K3ABKAP in conditions 1) and 2). (*J*) Bar graphs 1 and 2: Quantification of processive TMR-KIF3ABKAP events in the presence of APC-Alexa647 or APC-Alexa647 and KIF5AA. Bar graphs 3 and 4: Quantification of processive TMR-KIF3ABKAP events alone and in the presence of KIF5AA. The statistical significance was evaluated with unpaired, two-tailed *t* tests. (*K*) Confinement ratios of TMR-KIF3ABKAP alone, TMR-KIF3ABKAP + KIF5AA, TMR-KIF3ABKAP + APC-Alexa647 + β2Btub$_{wt}$ and TMR-KIF3ABKAP + APC-Alexa647 + β2Btub$_{wt}$ + KIF5AA (*L*) Scatter plot of track mean velocities of TMR-K3ABKAP in conditions 1) and 2) as well as TMR-K3ABKAP alone and together with KIF5AA. For *J–L* Statistical significance was evaluated with unpaired Mann–Whitney tests.

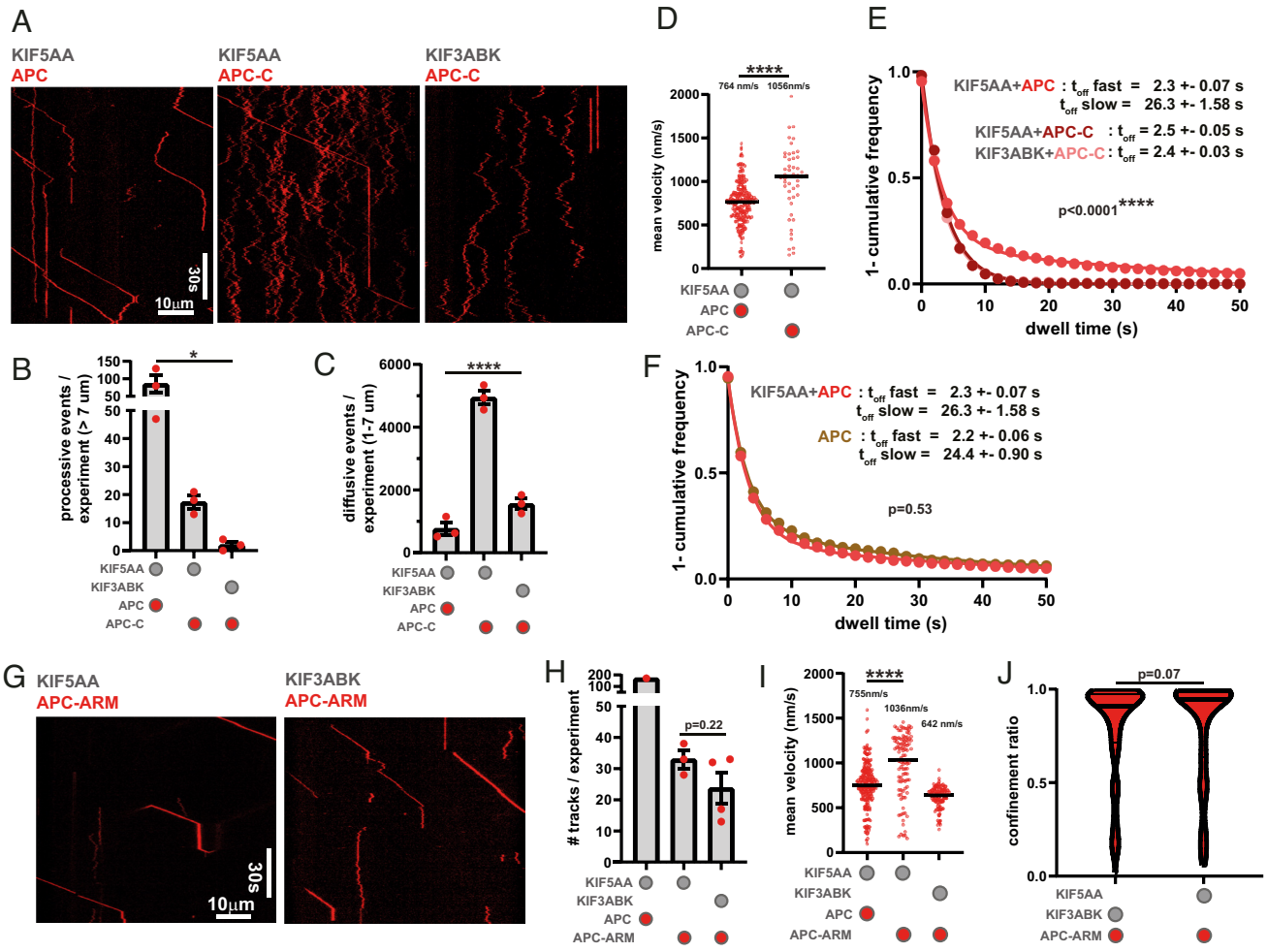

Fig. 4. KIF5AA interacts with the APC N- and C-termini. (*A*) Kymographs showing motion behavior of full-length APC-647 (25 pM) and APC-C-647 (25 pM) in the presence of KIF5AA (150 pM) or KIF3ABK (500 pM). (*B* and *C*) Quantification of processive (*B*) and diffusive events (*C*). Statistical significance was evaluated with one-way ANOVA tests. (*D*) Track mean velocities of full-length APC-647 and APC-C-647 transported by KIF5AA. Statistical significance was evaluated with an unpaired, two-tailed *t* test. (*E*) 1-cumulative frequency plot for the determination of diffusive full-length APC-647 and APC-C-647 in the presence of KIF5AA or KIF3ABK. Only events with a track displacement > 1 µm and a maximum distance < 7 µm were considered. Experimental data of APC-C-647 were fitted with a one-phase decay curve, whereas full-length APC-647 was fitted with a two-phase decay curve. Statistical significance between APC-647 and APC-C-647 in the presence of KIF5AA was evaluated with a Mann–Whitney test. (*F*) 1-cumulative frequency plot comparing the dwell times of diffusive APC in the presence or absence of KIF5AA. Experimental data were fitted with two-phase decay curves. Statistical significance was evaluated with a Mann–Whitney test. (*G*) Kymographs showing motion behavior of APC–ARM-647 (100 pM) in the presence of KIF5AA (150 pM) or KIF3ABK (500 pM). (*H*) Quantification of processive events. Full-length APC-647 (100 pM) transported by KIF5AA serves as control similar to *B*. Statistical significance was evaluated with an unpaired, two-tailed *t* test. (*I*) Track mean velocities of full-length APC-647 and APC–ARM-647 transported by KIF5AA as well as APC–ARM-647 transported by KIF3ABK. Statistical significance was evaluated with an unpaired, two-tailed *t* test. (*J*) Confinement ratio of APC–ARM-647 in the presence of KIF5AA and KIF3ABK. Statistical significance was evaluated with a Mann–Whitney test.

that the dwell times of an "APC-only" condition are almost identical to those of the "KIF5AA+APC" condition (Fig. 4*F*), we can rule out convolutions caused by the presence of KIF5AA.

We finally asked whether in addition to KAP3, KIF5AA might also be able to bind the APC–ARM fragment. We found that although KIF5AA transports full-length APC with a higher efficiency, both KIF5AA and KIF3ABK can processively transport the APC–ARM fragment (Fig. 4 *G* and *H*). Intriguingly, as for APC-C, the velocity of KIF5AA-mediated APC–ARM transport was again higher compared to that of full-length APC (Fig. 4*I*). Also, the previously noted diffusive component in KIF3ABK-mediated transport of full-length APC (Fig. 1*D*) was largely removed when APC–ARM was transported (Fig. 4*J*). In summary, full-length APC likely binds MTs with an N- and a C-terminal MT-binding site which together affect APC transport by KIF3ABK and KIF5AA: upon removal of either APC terminus, the KIF5AA-based transport velocity of APC increases. Due to the direct interaction between both kinesins, we can currently not resolve whether both kinesins also compete for binding to the APC–ARM region in a dynamic equilibrium.

Transport APC–RNPs Can Assemble on the Microtubule. Neuronal mRNPs exhibit a random Lévy walk; while being nonmotile most of the time, mRNPs can diffuse and exhibit bidirectional transport (45). Such a movement pattern can improve target site finding of randomly located objects (46). A mechanism in which kinesin motors push or drag MT lattice-diffusing APC–RNPs would thus offer an attractive framework for interpreting neuronal mRNP movements. We investigated the movements of Alexa-647-labeled KIF5AA and TMR-labeled APC in dual color TIRF-M experiments and found examples in which KIF5AA and APC landed simultaneously on MTs, indicating transport RNP assembly before MT binding (Fig. 5*A*, magnified frame on the middle right). Strikingly, we also observed that faster-moving KIF5AA encounters lattice-diffusing APC (Fig. 5*A* and Movie S5). We observed that the motor is able to

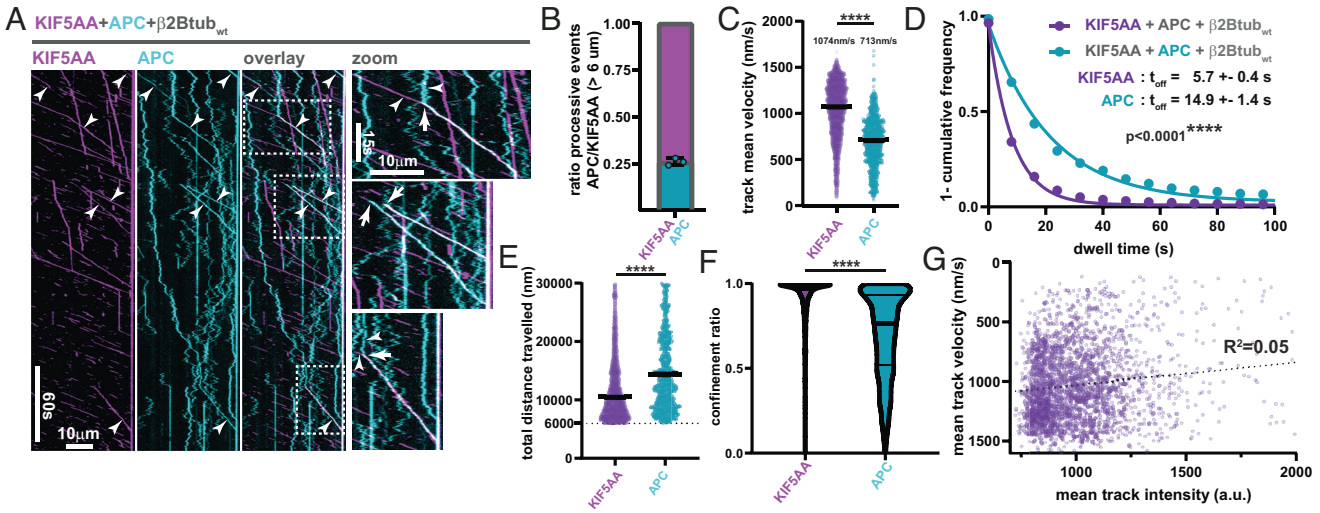

Fig. 5. APC changes KIF5AA motility parameters. (*A*) Kymographs showing the motion behavior of KIF5AA-647 (80 pM) in magenta and APC–TMR (50 pM) in cyan. APC–TMR transported by KIF5AA appears white in the overlay of kymographs. White dotted rectangles indicate zoomed parts showing diffusive APC–TMR being picked up by KIF5AA-647 resulting in processive APC–TMR transport (*Top* and *Bottom*) as well as colanding events of APC–TMR and KIF5AA-647 also resulting in processive APC–TMR transport (*Middle*). (*B*) Ratio of processive KIF5AA-647 transporting APC–TMR. Only events > 6 µm were considered. (*C*) Track mean velocities of KIF5AA-647 and APC–TMR populations. Note that about 25% of processive KIF5AA-647 transports APC–TMR. Median velocities are indicated and statistical significance was evaluated with a Mann–Whitney test. (*D*) 1-cumulative frequency plot comparing dwell times of KIF5AA-647 and APC–TMR. Statistical significance was evaluated with a Mann–Whitney test. (*E*) Scatter plot depicting the total distance traveled of APC–TMR and KIF5AA-647. Statistical significance was evaluated with a Mann–Whitney test. (*F*) Violin plot depicting confinement ratios of KIF5AA-647 and APC–TMR. Statistical significance was evaluated with a Mann–Whitney test. (*G*) Scatter plot testing the correlation of KIF5AA-647 mean track velocity and mean track intensity. The dotted line represents simple linear regression. R^2 indicates R squared.

"pick up" lattice-diffusing APC for further transport (Fig. 5*A*, magnified frames on the right, top, and bottom), which creates RNP trajectories with stationary rest phases and processive run events, as observed in mammalian neurons (45, 47). Of note, once KIF5AA is loaded with its APC cargo, a decrease in KIF5AA velocity can be observed. Labeling of both KIF5AA and APC enabled us to calculate the ratio of processive APC transport events to processive KIF5AA events which was ~1:4 (Fig. 5*B*). Considering the high APC labeling ratio of approximately 80% and its propensity to form a dimer (24), we assume that at least one of the APC molecules in each dimer is labeled. Hence, the majority of KIF5AA run events can be considered "cargo-free" run events. We analyzed the motility parameters of APC and KIF5AA populations separately. Despite the expected ~25% overlap of both data sets, we found that the KIF5AA data showed a higher velocity, resembling the velocity of KIF5AA loaded with either RNA, FMRP, or APC fragment cargoes (Figs. 1 and 3), while the APC fraction was moving at the characteristic KIF5AA–APC complex velocity (Fig. 5*C*). At the same time, the processive APC data exhibited a 2.5-fold higher dwell time (Fig. 5*D*) than the cargo-free KIF5AA data, and KIF5AA-transported APC traveled several µm farther than KIF5AA alone (Fig. 5*E*), although with a greater diffusive component than that of KIF5AA movements (Fig. 5*F*). In principle, motor oligomerization by the dimeric APC could cause such changes in motile behavior. However, we found no correlation between measured KIF5AA signal intensity and velocity (Fig. 5*G*). Thus, motor oligomerization by APC is unlikely the underlying reason for APC-induced motor slowdown.

In summary, these data support a mechanism in which the long dwell time of APC on the microtubule promotes encounters with KIF5AA which on its own binds only briefly, exhibiting short directional runs. Once KIF5AA–APC complexes assemble on the microtubule, KIF5AA is slowed down but becomes more processive. As these changes in motile behavior are not correlated with oligomerization of the motor protein and do not occur when any other cargo tested here is transported, we conclude that the simultaneous interaction of APC dimers with the MT and motor likely causes this effect on motor activity.

APC–RNPs Track Growing and Shrinking Microtubule Ends. APC is an EB-dependent microtubule plus-end-tracking protein (30) and APC-dependent mRNA localization to protrusions of axonal growth cones and NIH/3T3 cells were shown to be of crucial importance for polarization and migration (4, 39). We hence asked whether APC could also recruit mRNAs to polymerizing microtubule plus ends in addition to being an mRNA-motor adaptor. We purified EB1 and EB1-mGFP (*SI Appendix*, Fig. S4*A*) and initially used an in vitro TIRF-M assay with dynamically growing MTs to assess the dynamic behavior of EB1 and APC. We observed robust, EB1-dependent APC tracking of growing microtubule ends (Fig. 6*A* and Movie S6). Unexpectedly, APC could also track shrinking MT ends. As EB proteins recognize a GTP hydrolysis-dependent tubulin structure that occurs only during MT assembly, they cannot track depolymerizing microtubule ends (18, 19, 48). Hence, APC tracks shrinking MT ends independently of EB1 (Fig. 6*A*). The high-affinity interaction between EB1 and APC in solution could further be confirmed with SPR measurements, showing multisite binding on both the full APC C-terminus ("APC-C", residues 2,163 to 2,845) and the APC-basic domain alone (APC residues 2,163 to 2,670, *SI Appendix*, Fig. S4 *A–D*). This confirms that the C-terminal half of APC contains multiple EB-binding sites as predicted by the presence of six extended EB-binding SXIP motifs (49) in this region. We employed automated tracking of EB1-mGFP to determine MT growth speed and time of extension periods (*SI Appendix*, Fig. S4*E* and Movie S7). Under our experimental condition, the presence of APC had no effect on MT growth speed or the extension period of a polymerizing microtubule (Fig. 6*B*). Addition of β2tub$_{wt}$ RNA resulted in plus-end-tracking of APC–RNPs (Fig. 6*C* and Movies S8 and S9), with APC–RNPs also being able to track EB1-free, shrinking MTs (Fig. 6*C*). Of note, the addition of RNA had no effect

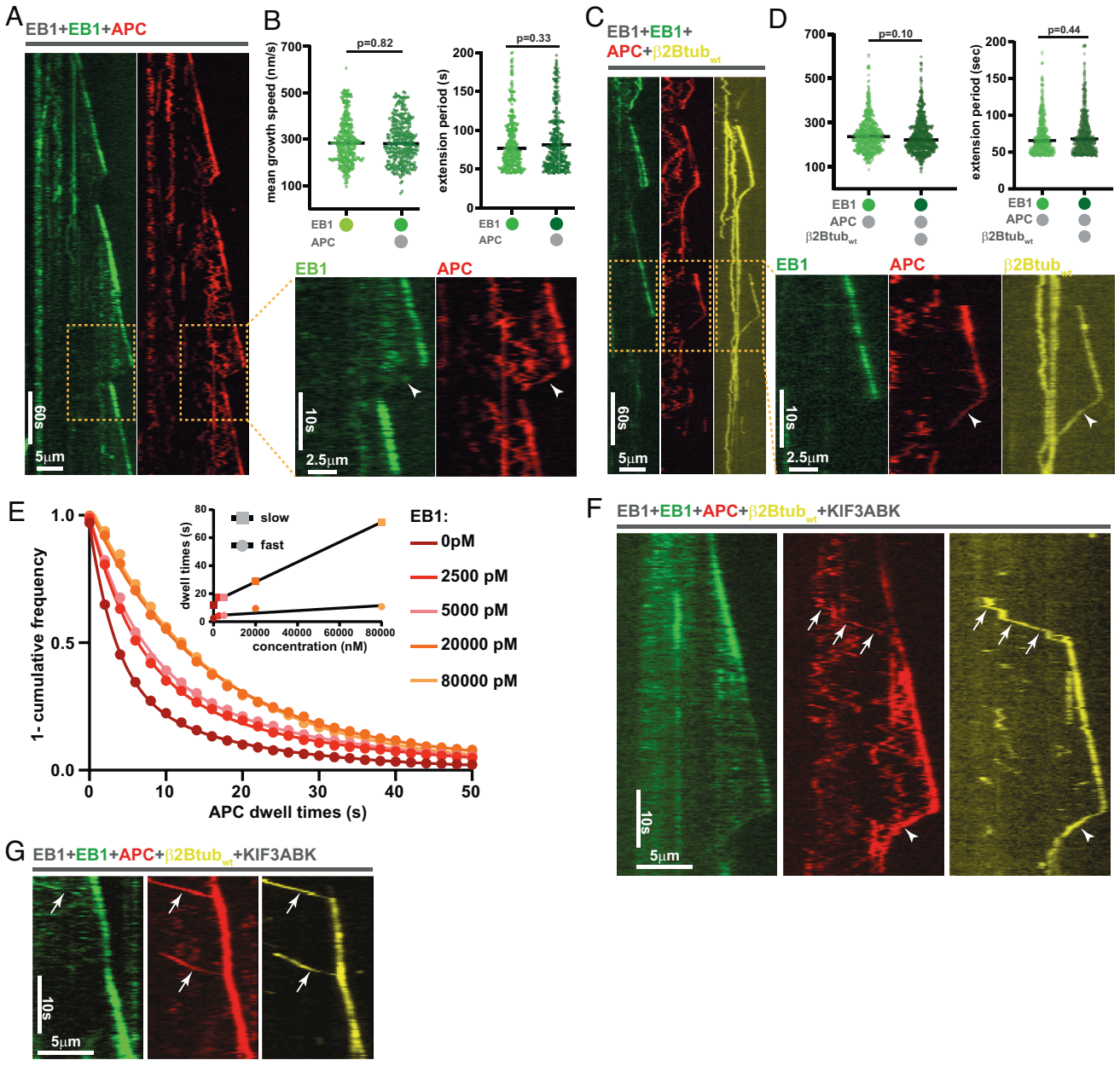

Fig. 6. Microtubule dynamics enable bidirectional movement of APC–RNPs. (*A*) Kymographs showing full-length APC-647 (400 pM) tracking growing and shrinking microtubule plus ends decorated with EB1-mGFP (5,000 pM) and unlabeled EB1 (5,000 pM). Yellow box indicates zoomed part. Arrowheads highlight APC-647 on shrinking MT plus end. (*B*) Microtubule growth speed and extension periods in the presence and absence of APC-647 measured by tracking EB1-mGFP. (*C*) Kymographs showing RNP complexes of APC-647 (400 pM) and TMR-β2tub$_{wt}$ (12,000 pM) tracking growing and shrinking microtubule plus ends decorated with EB1-mGFP (5,000 pM) and unlabeled EB1 (5,000 pM). Yellow box indicates zoomed part. Arrowheads highlight APC-647 and TMR-β2tub$_{wt}$ on shrinking MT plus end. (*D*) Microtubule growth speed and extension periods in the presence and absence of an APC-647–TMR-β2tuB$_{wt}$ complex measured by tracking EB1-mGFP. (*E*) 1-cumulative frequency plot showing dwell time of APC-647 (50 pM) on paclitaxel-stabilized MTs dependent on EB1 concentration. Experimental data were fitted with a two-phase decay model. Inset: Slow and fast half-lives of dwell times were plotted against EB1 concentrations. (*F* and *G*) Kymographs showing processive RNP complexes of APC-647 (400 pM) and TMR-β2tub$_{wt}$ (12,000 pM) in the presence of KIF3ABK (4,000 pM), EB1-mGFP (5,000 pM) and unlabeled EB1 (5,000 pM). Three distinct stages are depicted: i) processive transport of RNPs towards the growing MT plus end (arrows in *G* and *H*), ii) growing plus-end-tracking of RNPs in the presence of EB1-mGFP (*G* and *H*), iii) shrinking plus-end-tracking of RNPs in the absence of EB1-mGFP (arrowheads in *G*).

on MT growth speed or extension period (Fig. 6*D*). Control experiments show that APC–RNA complexes cannot track MT plus ends in the absence of EB1 (Movie S10) and that RNA is recruited to MT plus ends in an APC-dependent manner (Movie S11). Given the high-affinity interaction between EB1 and APC, we asked next whether EB1 can affect the dwell time of APC on MTs. We found that both the fast and the slow components of the APC dwell time on paclitaxel stabilized MTs increase with EB1 concentration to values of > 60 s (Fig. 6*F*). The long APC dwell times, even in the absence of EB1, are sufficient to enable processive shrinking-end-tracking of APC–RNA complexes, as APC dwell times can well extend beyond the duration of an MT shrinking event. Upon the addition of KIF3ABK, we observe bidirectional APC–RNA complex movements along MTs (Fig. 6 *G* and *H*), caused by kinesin-dependent, plus-end directed transport and the shrinking-end-tracking behavior of APC, potentially enabling mRNPs to enter and scan through fine cell protrusions and facilitate mRNA-target site finding by repeated and alternating cycles of MT plus- and minus-end-tracking with active transport (Movie S12).

Discussion

In this work, we show that APC–RNPs can be transported not only by the heterotrimeric kinesin-2 KIF3ABK, as previously shown (Baumann et al. 2020)*** but also by the homodimeric kinesin-1 KIF5AA. Compared to KIF3ABK, however, KIF5AA is less specific with weaker binding activities also to the β2tub RNA. These weaker interactions of KIF5A with mRNP components are one possible cause of the often-observed remaining transport activity which persists after a key mRNA transport factor has been disabled (27, 47, 50).

We further show that APC is a versatile adaptor that specifically binds several G-rich motifs of localized neuronal mRNAs with high affinity and low off rates. Of note, FMRP binds the same motifs as APC, partially with higher affinities, which suggests a competition for the same mRNA targets, likely being controlled by relative subcellular protein abundance and PTMs in cells. For instance, phosphorylation of APC by GSK3β modulates the APC–MT interaction (51). Given that the MT- and RNA-binding regions overlap, a similar mechanism for APC–RNA binding might exist.

While KIF3ABK binds the ARM region of APC (*SI Appendix*, Fig. S1*A*) via KAP3, KIF5A was reported to recognize a C-terminal APC fragment (Ruane et al., 2016 (25) and *SI Appendix*, Fig. S1*A*). This caused us to speculate that both kinesins can bind APC simultaneously, potentially increasing APC–RNP processivity. However, we could not detect any synergistic effect on APC transport parameters at limiting APC concentrations and in the presence of both kinesins. We rather find that all motility parameters except for the confinement ratio of APC in the presence of KIF3ABK and KIF5AA (scenario 2) are in between the parameters of the single motor conditions (scenarios 1 and 3). Specifically, the bimodal velocity distribution in the mixed motor condition argues for the presence of two distinct APC–kinesin populations and the mutually exclusive binding of KIF3ABK and KIF5AA to APC. Both motors might compete for the APC–ARM region, even though a more precise mapping of their exact interaction site is needed to support this scenario. As we found that both kinesins interact at least in the absence of cargo, it is currently not possible to construct a final model of what happens if both kinesins encounter APC; we can just exclude a synergistic scenario in which both kinesins would engage simultaneously to transport APC.

We observed that the velocity of KIF5AA-based transport of APC fragments, β2tub RNA, and FMRP is faster than the transport of full-length APC. As this happens at experimental conditions under which mostly a dimeric APC binds a single KIF3ABK, and the velocity of KIF5AA–APC complexes does not correlate with motor intensity, we exclude the possibility that motor oligomers cause the velocity difference. We instead propose that full-length APC and APC–RNPs might use a special transport mode in which APC remains in contact with the MT while the motor drags it along the lattice. This idea is also supported by the extended dwell time of KIF5AA–APC complexes compared to cargo-free KIF5AA, which argues for additional MT attachment sites provided by APC. Such a transport mechanism could have advantages for long-range transport; if the components of the transport complex were not "lost" freely diffusing in the cytoplasmic space, the diffusion of one or both components along the MT could facilitate the assembly of a transport complex. Further support for such a dragging transport mode comes from the observation, that lattice-diffusing APC can be "picked up" by KIF5AA but also slows the motor down at the moment of transport complex formation. We note that "pick up" events are observable in each experiment, but we refrain from statistical analysis as labeling both motor and cargo lowers the cargo-transport frequency which adds uncertainty about the true frequency at which such events can occur.

We finally show that EB1 is sufficient for recruiting APC and APC–RNPs to growing MT ends in vitro and that APC and APC–RNPs can track shrinking MT ends. Due to the high dwell times of full-length APC on the MT lattice, the observed shrinking-end-tracking is very likely caused by a continuous movement of APC–RNPs and not a rapid turnover as for EB proteins on the structural cap of MT plus ends (18, 19). Since APC localizes to MT plus ends within filopodia of axonal growth cones (39), the combined action of active transport and growing- and shrinking-MT plus end tracking could be an attractive mechanism to navigate bidirectionally within the growth cones and filopodia to scan for mRNP target sites.

As a microtubule plus-end-tracking protein, APC can further reach high local concentrations around growing MT ends, which could also contribute to a concentration-driven displacement of other proteins binding to similar mRNA motifs such as FMRP. As FMRP functions as a translational repressor (42), such a plus-end-tracking-driven remodeling of mRNPs would be an interesting mechanism to promote the translation of mRNAs from translationally inactive transport mRNPs upon their delivery to cellular domains with highly dynamic MTs, e.g., axonal growth cones. A plus-end-trailing of mRNPs has been observed in axonal growth cones (16), and it will now be of the highest interest to understand which function interactions of mRNPs with growing MT ends could serve in the cell.

Materials and Methods

Materials. Chemicals were obtained from Sigma if not stated otherwise. Single-fluorophore, 5′-end-labeled RNA fragments from mouse β-actin mRNA (accession number: NM_007393.5) and mouse β2-tubulin-mRNA (accession number: NM_023716.2) were purchased from IBA-Lifesciences (Germany). All 25 nt RNAs used for SPR experiments were purchased from IDT. The fragments for β-actin and β2tub mRNAs were taken from the same transcripts listed above. The Map1b-fragment comes from accession number NM_008634.2, the Camk2α-mRNA fragment from NM_001286809.1. TIRF-M experiments were performed on an iMIC (TILL Photonics, Germany) TIRF microscope equipped with three Evolve 512 EMCCD cameras (Photometrics, UK), a 100× 1.49 NA objective lens (Olympus, Japan), a quadband filter (405/488/561/647, Semrock, USA), and four different laser lines (405 nm, 488 nm, 561 nm, and 639 nm). An Olympus tube lens adds a post magnification of ×1.33, which results in a final pixel size of 120.3 nm. SPR experiments were performed on a BIACORE T100 system (GE Healthcare) using the Twin-Strep-tag® Capture Kit (IBA-Lifesciences) and CM5-Chips (Cytiva).

Methods. All proteins used in this work were either expressed in E.coli, SF9, or SF21 insect cells. Proteins were purified with a combination of affinity and size-exclusion chromatography. SNAP labeling was used for fluorescent labeling of proteins. All proteins and RNAs were stored as single-use aliquots in liquid nitrogen until immediately prior to the assembly of the assay mixtures.

All reconstitution and microscopy experiments were essentially performed as described before (24, 31).

Motility data of RNA–protein complexes were analyzed using the TrackMate plugin (52) for Fiji (53). Please see *SI Appendix, Methods* for details.

Data, Materials, and Software Availability. All data needed to evaluate the conclusions in the paper are present in the paper and/or the *SI Appendix*.

ACKNOWLEDGMENTS. We thank Thomas Surrey and Davide Normanno for their continuous support by giving us access to their microscope equipment and assisting with equipment-related technical issues throughout the entire project. We also thank the CRG BMS-PT core facility for its support by providing reagents and training on instrumentation. Funding: This work was funded by the Spanish

Ministry of Economy and Competitiveness (MINECO) [BFU2017-85361-P], [PID2020-114870GB-I00], [BFU2015-62550-ERC], the Ministerio de Ciencia, Innovación y Universidades and Fondo Social Europeo (FSE) [PRE2018-084501], Juan de la Cierva-Incorporación Program [IJCI-2015-25994], the Human Frontiers in Science Program (HFSP) [RGY0083/2016], and the European Research Council (ERC) [H2020-MSCA-IF-2014-659271.]. We further acknowledge the support of the Spanish Ministry of Economy and Competitiveness, 'Centro de Excelencia Severo Ochoa' [SEV-2012-0208].

Author affiliations: [a]Centre for Genomic Regulation, The Barcelona Institute of Science and Technology, Barcelona 08003, Spain; and [b]Universitat Pompeu Fabra, Barcelona 08002, Spain

1. C. H. Coles, F. Bradke, Microtubule self-organization via protein-RNA network crosstalk. *Cell* **158**, 245–247 (2014).
2. P. Litman, J. Barg, L. Rindzoonski, I. Ginzburg, Subcellular localization of tau mRNA in differentiating neuronal cell culture: implications for neuronal polarity. *Neuron* **10**, 627–38 (1993).
3. E. H. Kislauskis, X. Zhu, R. H. Singer, Beta-Actin messenger RNA localization and protein synthesis augment cell motility. *J. Cell Biol.* **136**, 1263–1270 (1997).
4. S. Mili, K. Moissoglu, I. G. Macara, Genome-wide screen reveals APC-associated RNAs enriched in cell protrusions. *Nature* **453**, 115–119 (2008).
5. K. Moissoglu *et al.*, RNA localization and co-translational interactions control RAB 13 GTP ase function and cell migration. *EMBO J.* **39**, e104958 (2020).
6. M. Batish, P. van den Bogaard, F. R. Kramer, S. Tyagi, Neuronal mRNAs travel singly into dendrites. *Proc. Natl. Acad. Sci. U.S.A.* **109**, 4645–4650 (2012).
7. H. Y. Park *et al.*, Visualization of dynamics of single endogenous mRNA labeled in live mouse. *Science* **343**, 422–424 (2014).
8. G. Wang *et al.*, Spatial organization of the transcriptome in individual neurons. bioRxiv [Preprint] (2020). https://doi.org/10.1101/2020.12.07.414060. (Accessed 8 December 2020).
9. A. R. Buxbaum, G. Haimovich, R. H. Singer, In the right place at the right time: visualizing and understanding mRNA localization. *Nat. Rev. Mol. Cell Biol.* **16**, 95–109 (2015).
10. G. Tushev *et al.*, Alternative 3′ UTRs modify the localization, regulatory potential, stability, and plasticity of mRNAs in neuronal compartments. *Neuron* **98**, 495–511.e6 (2018).
11. B. Y. Monroy *et al.*, A combinatorial MAP code dictates polarized microtubule transport. *Dev. Cell* **53**, 60–72.e4 (2020).
12. C. Janke, M. M. Magiera, The tubulin code and its role in controlling microtubule properties and functions. *Nat. Rev. Mol. Cell Biol.* **21**, 307–326 (2020).
13. L. C. Kapitein, C. C. Hoogenraad, Building the neuronal microtubule cytoskeleton. *Neuron* **87**, 492–506 (2015).
14. E. C. Rodrigues, J. Grawenhoff, S. J. Baumann, N. Lorenzon, S. P. Maurer, mammalian neuronal mRNA transport complexes: The few knowns and the many unknowns. *Front. Integr. Neurosci.* **15**, 1–8 (2021).
15. T. J. Messitt *et al.*, Multiple kinesin motors coordinate cytoplasmic RNA transport on a subpopulation of microtubules in Xenopus oocytes. *Dev. Cell* **15**, 426–436 (2008).
16. K.-M. Leung *et al.*, Cue-polarized transport of β-actin mRNA depends on 3′UTR and microtubules in live growth cones. *Front. Cell. Neurosci.* **12**, 300 (2018).
17. H.H.-W. Wong *et al.*, RNA docking and local translation regulate site-specific axon remodeling in vivo. *Neuron* **95**, 852–868.e8 (2017).
18. P. Bieling *et al.*, Reconstitution of a microtubule plus-end tracking system in vitro. *Nature* **450**, 1100–1105 (2007).
19. S. P. Maurer, F. J. Fourniol, G. Bohner, C. A. Moores, T. Surrey, EBs recognize a nucleotide-dependent structural cap at growing microtubule ends. *Cell* **149**, 371–382 (2012).
20. B. Feierbach, F. Verde, F. Chang, Regulation of a formin complex by the microtubule plus end protein tea1p. *J. Cell Biol.* **165**, 697–707 (2004).
21. A. Akhmanova, M. O. Steinmetz, Tracking the ends: A dynamic protein network controls the fate of microtubule tips. *Nat. Rev. Mol. Cell Biol.* **9**, 309–322 (2008).
22. J. van Haren *et al.*, Dynamic microtubules catalyze formation of navigator-TRIO complexes to regulate neurite extension. *Curr. Biol.* **24**, 1778–1785 (2014).
23. S. G. Martin, F. Chang, Cell polarity: A new mod (e) of anchoring microtubules play a central role in the establishment. *Curr. Biol.* **13**, 711–713 (2003).
24. S. Baumann *et al.*, A reconstituted mammalian APC-kinesin complex selectively transports defined packages of axonal mRNAs. *Sci. Adv.* **6**, eaaz1588 (2020).
25. P. T. Ruane *et al.*, Tumour suppressor adenomatous polyposis coli (APC) localisation is regulated by both Kinesin-1 and Kinesin-2. *Sci. Rep.* **6**, 27456 (2016).
26. E. A. Scarborough *et al.*, Microtubules orchestrate local translation to enable cardiac growth. *Nat. Commun.* **12**, 1547 (2021).
27. J. B. Dictenberg, S. A. Swanger, L. N. Antar, R. H. Singer, G. J. Bassell, A direct role for FMRP in activity-dependent dendritic mRNA transport links filopodial-spine morphogenesis to fragile X syndrome. *Dev. Cell* **14**, 926–939 (2008).
28. Y. Kanai, N. Dohmae, N. Hirokawa, Kinesin transports RNA. *Neuron* **43**, 513–525 (2004).
29. L. K. Su *et al.*, APC binds to the novel protein EB1. *Cancer Res.* **55**, 2972–2977 (1995).
30. Y. Mimori-Kiyosue, N. Shiina, S. Tsukita, The dynamic behavior of the APC-binding protein EB1 on the distal ends of microtubules. *Curr. Biol.* **10**, 865–868 (2000).
31. J. Grawenhoff, S. Baumann, S. P. Maurer, In vitro reconstitution of kinesin-based axonal mRNA transport. *Methods Mol. Biol.* **2431**, 547–568 (2022).
32. P. Bieling, I. A. Telley, C. Hentrich, J. Piehler, T. Surrey, "Fluorescence microscopy assays on chemically functionalized surfaces for quantitative imaging of microtubule, motor, and +TIP dynamics" in *Methods in Cell Biology* (Elsevier, 2010),vol. **95**, pp. 555–580.
33. E. Meijering, O. Dzyubachyk, I. Smal, Methods for cell and particle tracking. *Methods Enzymol.* **504**, 183–200 (2012).
34. L. Dimitrova-Paternoga *et al.*, Molecular basis of mRNA transport by a kinesin-1–atypical tropomyosin complex. *Genes Dev.* **35**, 976–991 (2021).
35. J. Zhao *et al.*, Specific depletion of the motor protein KIF5B leads to deficits in dendritic transport, synaptic plasticity and memory. *Elife* **9**, 1–34 (2020).
36. B. Y. Monroy *et al.*, Competition between microtubule-associated proteins directs motor transport. *Nat. Commun.* **9**, 1–12 (2018).
37. P. J. Hooikaas *et al.*, MAP7 family proteins regulate kinesin-1 recruitment and activation. *J. Cell Biol.* **218**, 1298–1318 (2019).
38. L. S. Ferro, Structural and functional insight into regulation of kinesin-1 by microtubule-associated protein MAP7. *Science* **37**, 326–331 (2022).
39. N. Preitner *et al.*, APC is an RNA-binding protein, and its interactome provides a link to neural development and microtubule assembly. *Cell* **158**, 368–382 (2014).
40. J. C. Darnell *et al.*, Fragile X mental retardation protein targets G quartet mRNAs important for neuronal function. *Cell* **107**, 489–499 (2001).
41. R. Goering *et al.*, FMRP promotes RNA localization to neuronal projections through interactions between its RGG domain and G-quadruplex RNA sequences. *Elife* **9**, 784728 (2020).
42. J. C. Darnell *et al.*, FMRP stalls ribosomal translocation on mRNAs linked to synaptic function and autism. *Cell* **146**, 247–261 (2011).
43. A. Reilein, W. J. Nelson, APC is a component of an organizing template for cortical microtubule networks. *Nat. Cell Biol.* **7**, 463–73 (2005).
44. T. Jimbo *et al.*, Identification of a link between the tumour suppressor APC and the kinesin superfamily. *Nat. Cell Biol.* **4**, 323–327 (2002).
45. M. S. Song, H. C. Moon, J. H. Jeon, H. Y. Park, Neuronal messenger ribonucleoprotein transport follows an aging Lévy walk. *Nat. Commun.* **9**, 1–8 (2018).
46. G. M. Viswanathan *et al.*, Optimizing the success of random searches. *Nature* **401**, 911–914 (1999).
47. Y. J. Yoon *et al.*, Glutamate-induced RNA localization and translation in neurons. *Proc. Natl. Acad. Sci. U.S.A.* **113**, E6877–E6886 (2016).
48. S. P. Maurer, P. Bieling, J. Cope, A. Hoenger, T. Surrey, GTPgammaS microtubules mimic the growing microtubule end structure recognized by end-binding proteins (EBs). *Proc. Natl. Acad. Sci. U.S.A.* **108**, 3988–3993 (2011).
49. K. Jiang *et al.*, A proteome-wide screen for mammalian SxIP motif-containing microtubule plus-end tracking proteins. *Curr. Biol.* **22**, 1800–1807 (2012).
50. T. Sharangdhar *et al.*, A retained intron in the 3′-UTR of Calm3 mRNA mediates its Staufen2- and activity-dependent localization to neuronal dendrites. *EMBO Rep.* **18**, 1762–1774 (2017).
51. J. Zumbrunn, K. Kinoshita, A. A. Hyman, I. S. Näthke, Binding of the adenomatous polyposis coli protein to microtubules increases microtubule stability and is regulated by GSK3β phosphorylation. *Curr. Biol.* **11**, 44–49 (2001).
52. J. Y. Tinevez *et al.*, TrackMate: An open and extensible platform for single-particle tracking. *Methods* **115**, 80–90 (2017).
53. J. Schindelin *et al.*, Fiji: An open-source platform for biological-image analysis. *Nat. Methods* **9**, 676–682 (2012).